STXBP1 inhibits glioma progression by modulating ferroptosis and epithelial-mesenchymal transition

Keywords
Ferroptosis, Epithelial-mesenchymal transition, Glioma, STXBP1

Abstract

Introduction
This study investigates the role of STXBP1 in glioma, particularly its involvement in regulating ferroptosis and epithelial-mesenchymal transition (EMT), and examines its impact on glioma cell behavior.

Material and methods
Differential gene expression analysis was performed on a glioma dataset, and protein-protein interaction (PPI) network analysis identified genes with significant prognostic value. Least absolute shrinkage and selection operator (LASSO) Cox regression analysis further narrowed the scope. Key genes were obtained through nomogram analysis and expression verification was performed. In in vitro cell experiments, knockdown of STXBP1 was performed in glioma cell lines and the effects on cell proliferation, migration, invasion, cell cycle distribution, apoptosis, and markers of ferroptosis and EMT were assessed.

Results
After bioinformatics analysis, STXBP1 was identified as a hub gene, and in vitro cell experiments were performed. STXBP1 knockdown in glioma cells increased proliferation, migration, and invasion, altered cell cycle distribution (reducing S phase and increasing G1 phase), and decreased apoptosis. Ferroptosis markers showed elevated GPX4 expression and reduced 12-HETE and 15-HETE levels. Ferroptosis inducers (Sorafenib, erastin) heightened LDH release and reduced viability, while inhibitors (ferrostatin-1, U0126) had opposing effects. STXBP1 knockdown also reduced lipid peroxidation and mitigated the cytotoxic effects of Sorafenib, indicating a role in ferroptosis regulation. Additionally, STXBP1 knockdown impacted EMT markers, decreasing N-cadherin and Vimentin and increasing E-cadherin.

Conclusions
STXBP1 functions as a tumor suppressor in glioma, regulating ferroptosis and EMT. It presents potential as a therapeutic target in glioma management.

STXBP1 inhibits glioma progression by modulating ferroptosis and epithelial-mesenchymal transition

Xuemin Li1[#,*], Chonggong Zhang2[#], Peiyu Qian3[,#]
1.Putuo Hospital, Shanghai University of Traditional Chinese Medicine, No. 409, Meiling North Road, Caoyang, Putuo District, Shanghai, China, 200063.
2.13 Fudong Street, Taiyuan City, Shanxi Province, China. Neurosurgery Department of Shanxi Province Integrated Traditional and Western Medicine Hospital, 030001.
3. Institutes of Biomedical Sciences, Fudan University, Shanghai, 200032, China

# These authors contributed equally
*Corresponding author:
Xuemin Li , Dr
E-mail: xixi0348@126.com
Putuo Hospital, Shanghai University of Traditional Chinese Medicine, No. 409, Meiling North Road, Caoyang, Putuo District, Shanghai, China, 200063.

Abstract

Objective: This study investigates the role of *STXBP1* in glioma, particularly its involvement in regulating ferroptosis and epithelial-mesenchymal transition (EMT), and examines its impact on glioma cell behavior.

Methods: Differential gene expression analysis was performed on a glioma dataset, and protein-protein interaction (PPI) network analysis identified genes with significant prognostic value. Least absolute shrinkage and selection operator (LASSO) Cox regression analysis further narrowed the scope. Key genes were obtained through nomogram analysis, and expression verification was performed. In *in vitro* cell experiments, knockdown of *STXBP1* was performed in glioma cell lines. The effects on cell proliferation, migration, invasion, cell cycle distribution, apoptosis, and markers of ferroptosis and EMT were assessed.

Results: After bioinformatics analysis, *STXBP1* was identified as a hub gene, and *in vitro* cell experiments were performed. *STXBP1* knockdown in glioma cells increased proliferation, migration, and invasion, altered cell cycle distribution (reducing S phase and increasing G1 phase), and decreased apoptosis. Ferroptosis markers showed elevated *GPX4* expression and reduced 12-HETE and 15-HETE levels. Ferroptosis inducers (Sorafenib, erastin) heightened LDH release and reduced viability, while inhibitors (ferrostatin-1, U0126) had opposing effects. *STXBP1* knockdown also reduced lipid peroxidation and mitigated the cytotoxic effects of Sorafenib, indicating a role in ferroptosis regulation. Additionally, *STXBP1* knockdown impacted EMT markers, decreasing N-cadherin and Vimentin and increasing E-cadherin.

Conclusion: *STXBP1* functions as a tumor suppressor in glioma, regulating ferroptosis and EMT. It presents potential as a therapeutic target in glioma management.

Keywords: *STXBP1*, Ferroptosis, Epithelial-mesenchymal transition, Glioma

Running Title: *STXBP1* promotes glioma progression via ferroptosis and EMT

Introduction

Gliomas are common tumors that arise in the brain, and common subtypes include astrocytomas, oligodendrogliomas, and ependymoma(1). Glial tumors encompass a broader spectrum, including mixed gliomas, all derived from glial cells(2). These tumors can occur in different brain and spinal cord regions and exhibit different histological and molecular characteristics(3). The World Health Organization (WHO) system states that gliomas are classified histologically and graded for malignancy(4). Gliomas of grades I and II are regarded as low-grade, but those of grades III and IV are high-grade and significantly aggressive. High-grade gliomas develop swiftly and invade surrounding tissue, posing significant treatment challenges. The etiology of glioma is multifactorial and involves genetic predisposition, ionizing radiation, and environmental factors(5). Clinically, gliomas can cause headaches, seizures, cognitive deficits, and focal neurological deficits, depending on their location and size(6). Standard treatments include surgical resection, chemotherapy, and radiation therapy(7). Even with advancements in treatment, glioma patients still have a dismal prognosis, particularly those with malignancies of a high grade, because of their aggressive and recurrent nature(8). Research continues to investigate the underlying molecular processes of glioma formation and create novel therapeutic approaches to enhance patient outcomes.

Ferroptosis is a type of controlled cell death characterized by iron-dependent lipid peroxidation(9). Unlike apoptosis or necrosis, ferroptosis involves the collection of lipid reactive oxygen species (ROS), leading to membrane damage and cell death. It is crucial for several physiological functions, including immune response and tissue homeostasis. Dysregulation of ferroptosis is associated with several tumors, including glioma(10). Zhu M et al. utilized a biomimetic nanosonosensitizer for synergistic therapy against gliomas, combining sonodynamic therapy (SDT) and ferroptosis(11). This approach, facilitated by circulated microbubbles (MBs)and focusing ultrasound (US) to open the blood-brain barrier (BBB), resulted in a significant reduction in orthotopic gliomas. Additionally, Zhou L et al. identified the impact of ferroptosis on glioma prognosis, potentially regulated by autophagy(12). Their novel gene signature, incorporating autophagy-ferroptosis genes, predicts glioma survival and offers insights for future treatment strategies. Zheng Y et al. explored the importance of ferroptosis-related genes in prognosis in lower-grade gliomas (LGG), identifying 12 genes associated with overall survival in LGG patients(13). This implies a potential link between ferroptosis and LGG prognosis. Moreover, ferroptosis has been linked to epithelial-mesenchymal transition (EMT), a procedure that enhances tumor invasiveness and metastasis, suggesting a broader impact on cancer progression. For example, balsalazide induces ferroptosis via a Slug-dependent EMT signaling pathway, inhibiting the growth of glioblastoma (GBM)(14). The interplay between ferroptosis and EMT further underscores the complex molecular landscape of gliomas, offering new avenues for therapeutic intervention. Understanding the molecular mechanisms of ferroptosis provides a promising approach to the treatment of gliomas, highlighting its

relevance in developing innovative therapeutic strategies.

STXBP1, also designated Syntaxin Binding Protein 1, is a gene situated on chromosome 9q34.11 that encodes a protein of paramount importance for synaptic vesicle exocytosis(15). This protein is vital in regulating neurotransmitter release at synapses, particularly in the central nervous system. Mutations in the *STXBP1* gene have been linked to several neurological disorders, including intellectual disability and early infantile epileptic encephalopathy (EIEE)(9). These mutations result in the disruption of normal synaptic function, which in turn leads to the development of abnormal neuronal excitability and synaptic transmission. Research indicates that *STXBP1* mutations are associated with a spectrum of clinical phenotypes, ranging from severe epileptic encephalopathies to milder forms of developmental delay and intellectual disability. For example, Zhang Y et al. demonstrated significant pleiotropy between *STXBP1* and *SCN2A* across four neurodevelopmental disorders, suggesting the potential for shared genetic foundations(16). Zhou P et al. demonstrated a strong association between STXBP1 mutations and West syndrome in epileptic encephalopathies, underscoring the utility of targeted next-generation sequencing (NGS) for diagnosing genetic etiologies and assessing variant pathogenicity(17). Furthermore, Stamberger H et al. identified *STXBP1* mutations as a primary contributor to epilepsy and encephalopathy, often accompanied by severe to profound intellectual disability and various seizure types(18). A comprehensive understanding of the molecular processes underlying *STXBP1*-related diseases is essential for advancing targeted therapies and improving patient outcomes. This research continues to indicate the function of *STXBP1* in synaptic physiology and its impact on the pathogenesis of neurological diseases.

This study aims to investigate the function of *STXBP1* in glioma, particularly its involvement in regulating ferroptosis and EMT. Given its significant impact on neurological function and potential link to mechanisms of cancer progression, we aimed to elucidate the impact of *STXBP1* on the pathogenesis of glioma cells. Functional experiments targeting *STXBP1* clarified its roles in glioma cell migration, proliferation, invasion, apoptosis, cell cycle distribution, and regulation of ferroptosis. Furthermore, the study demonstrated the influence of *STXBP1* on the EMT of ferroptosis-dependent tumor cells, indicating its multifaceted involvement in tumor progression. Collectively, these results offer important new understandings of the molecular pathways underlying the growth of gliomas and possible targets for therapeutic intervention.

Materials and methods

Download of glioma-related data sets and screening of differentially expressed genes (DEGs)

Glioma microarray data sets, including GSE12657, GSE16011, and GSE41031, were retrieved from the Gene Expression Omnibus (GEO) database (https://www.ncbi.nlm.nih.gov/gds/). Among them, the GSE12657 dataset contains 14 glioma samples and 5 control samples, the GSE16011 dataset contains 276 glioma

samples and 8 control samples, and the GSE41031 dataset contains 3 glioma samples and 3 control samples. Additionally, the Cancer Genome Atlas (TCGA)-glioma dataset was obtained via the ASSISTANT for Clinical Bioinformatics website (https://www.aclbi.com/static/index.html#/), comprising 666 glioma samples and 5 normal control samples. The probe ID was translated into gene symbols, and differential analysis was employed by the Limma package in the R programming language (http://www.r-project.org). Genes with fold change (FC) > 2 were regarded as DEGs that were upregulated, genes with FC < 0.5 were considered as down-regulated DEGs, and the statistical significance level was set at p-value < 0.05.

Cross-analysis and prognostic assessment of overlapping DEGs in glioma datasets

The upregulated and downregulated DEGs from TCGA-glioma, GSE12657, GSE16011, and GSE41031 datasets were subjected to cross-analysis using the bioinformatics platform (https://bioinformatics.psb.ugent.be/webtools/Venn/). Overlapping upregulated and downregulated DEGs were obtained. Subsequently, protein-protein interaction (PPI) network analysis was used on overlapping DEGs utilizing the Search Tool for the Retrieval of Interacting Genes (STRING) database (https://string-db.org/). The generated PPI network included parameters such as degree, Edge Percolated Component (EPC), and Maximum Neighborhood Component (MNC), and was displayed using Cytoscape, an open-source network visualization program (version 3.7.1). The statistical significance of the obtained results was evaluated, with a significance threshold set at $p < 0.05$. Cross-analysis of the top 25 genes based on degree, MNC, and EPC yielded key overlapping genes. To assess the prognostic significance of the identified genes, we used an overall survival (OS) analysis utilizing the Cox proportional hazards model. The 95% confidence intervals (CIs)and hazard ratios (HRs) for each gene were calculated, and genes with significant p-values ($p < 0.05$) were considered prognostically relevant.

Identification of characteristic prognostic genes and construction of the risk prognostic model

The analysis of significant genes for OS prognosis was completed utilizing the "glmnet" package in R software. The tuning parameters for the Least Absolute Shrinkage and Selection Operator (LASSO) model in the glmnet program (https://CRAN.R-project.org/package=glmnet) were determined through ten-fold cross-validation. The optimal λ, representing the minimum criterion for adjusted parameters, was identified to select the most predictive genes. These selected genes, representing the most statistically significant predictors in our dataset, formed the foundation of the risk prognostic model. Subsequently, the glioma cohort from the TCGA database was stratified into two risk groups (high-risk and low-risk) according to the expression patterns of the relevant genes. A risk assessment was then conducted for both groups. Kaplan-Meier (KM) analysis was employed to ascertain the OS probability for the two risk groups. Additionally, median survival time was calculated, and the statistical significance of survival differences between the two groups was assessed using the log-rank test to derive p-values. Hazard ratios (HR) for the high-risk group were also

computed to further elucidate relative risk. Finally, Receiver Operating Characteristic (ROC) curves were generated using the "timeROC" package, and the Area Under Curve (AUC) values were computed to assess the predictive ability of the prognostic models for patient survival at 1, 3, and 5 years. Higher AUC values indicate stronger prognostic prediction capabilities.

Identification of hub genes in glioma

Prognostic feature genes of significance were subjected to correlation analysis utilizing the R package. Multivariate and univariate Cox regression examinations were conducted on signature genes and specific clinical predictive variables (age, grade stage) using the forestplot program (https://CRAN.R-project.org/package=forestplot). The 95% CIs, HRs, and *p*-values were calculated for each variable, identifying key prognostic factors with a p-value < 0.05. Subsequently, nomograms predicting 1-, 3-, and 5-year survival were built with the "rms" package (https://CRAN.R-project.org/package=rms), and the concordance index (C-index) was determined. Calibration curves were generated to assess the nomogram's predictive performance, with closer alignment between the survival curves and the calibration curve indicating better model performance. To evaluate the expression of the three signature genes, processing and displaying data were executed with R (version 4.1.2), examining their expression in tumor and normal groups across the TCGA-glioma, GSE12657, GSE16011, and GSE41031 datasets.

Cell sources and processing

Human embryonic brain cells (HEB) and Glioma cells, including U251, SW1783, and U87, were purchased from the Chinese Academy of Sciences (Shanghai, China), kept in Dulbecco's Modified Eagle Medium (DMEM) with 1% penicillin-streptomycin and 10% fetal bovine serum (FBS) added. Cell cultures were maintained in a humidified atmosphere at 37°C with 5% CO_2. For the ferroptosis experiments, glioma cells were planted at a density of 1×10^6 cells per well in 6-well plates. The cells were treated with the following compounds for 3 days: Sorafenib (5 μM) and erastin (10 μM) were used as ferroptosis inducers, while ferrostatin-1 (1 μM) and U0126 (5 μM) were used as ferroptosis inhibitors. Dimethyl sulfoxide (DMSO) at a concentration of 5 μM was used as a control. Sorafenib and erastin promoted lipid peroxidation, leading to cell death, whereas ferrostatin-1 and U0126 prevented lipid peroxidation, thereby protecting the cells. This experimental setup allowed for the evaluation of the impacts of ferroptosis modulation on glioma cell viability and the associated molecular pathways.

Cell transfection

For transient transfection, glioma cells were seeded at a density of 2×10^5 cells per well in 24-well plates. Specific small interfering RNAs (siRNAs) targeting *STXBP1* (si-*STXBP1*-1, si-*STXBP1*-2, and si-*STXBP1*-3) were used to knock down *STXBP1* expression in the glioma cells. As a control, cells were transfected with a non-targeting siRNA (si-NC). Cells were transfected utilizing Lipofectamine 3000 (Invitrogen, China) in compliance with the manufacturer's guidelines. Following transfection, the cells were

incubated for a specific duration to ensure efficient knockdown of STXBP1 expression.

Quantitative real-time polymerase chain reaction (qRT-PCR)

The total RNA of glioma cells was extracted by the TRIzol reagent (Tiangen, Beijing, China) as directed by the manufacturer. For cDNA synthesis, we utilized a PrimeScript RT kit from Dalian, China. To do qRT-PCR with the StepOnePlus Real-Time PCR System (Applied Biosystems, Shanghai, China), SYBR Green PCR Master Mix (Takara, China) was utilized. Gene expression of *STXBP1*, *GPX4*, *N-cadherin*, *E-cadherin*, and *Vimentin* were quantified and normalized to *GAPDH*. All target expression levels were computed with the $2^{-\Delta\Delta CT}$ technique. A set of primer sequences was found in Table 1.

Western blot (WB) assay

Phosphatase inhibitors (CoWin Biosciences, Nanjing, China) were included in RIPA lysis buffer (Solarbio, Beijing, China), which was used to generate protein lysates from glioma cells. The BCA Protein Assay Kit (Beyotime, China) was employed to measure the protein concentration. Proteins in equal quantities were separated using 10% SDS-PAGE and then put onto PVDF membranes (Beyotime, Beijing, China). Primary antibodies were incubated on membranes that had been blocked with 5% skim milk, including anti-STXBP1, anti-CDK-1, anti-Cyclin B1, anti-Cyclin A2, anti-GPX4, anti-N-cadherin, anti-E-cadherin, and anti-Vimentin (Wuhan Sanying Biology Technology Co., Ltd.), at a dilution of 1:2000. GAPDH (Kangcheng, Shanghai, China, 1:5000) was used as an internal reference. After washing, the corresponding secondary antibodies (1:5000 dilution) coupled with horseradish peroxidase (HRP) were incubated on the membranes for 1 hour at room temperature. An enhanced chemiluminescence (ECL) kit (Tiangen, Beijing, China) was used to visualize the protein bands, and a ChemiDoc imaging equipment (Bio-Rad, Shanghai, China) was used to take the images.

Cell counting kit-8 (CCK-8) assay

The CCK-8 aassay (KeyGEN, Nanjing, China) was used to evaluate the vitality of the glioma cells. In 96-well plates, glioma cells were planted at a density of 5×10^3 cells per well. After adding CCK-8 reagent to each well after treatment, a microplate reader (Kehua Technologies, Inc., Shanghai, China) was employed to detect the absorbance at 450 nm after 24h, 48h, 72h, 96h, and 120h.

Cell invasion and migration assays

Transwell assays (Corning Inc., Corning, NY, USA) were employed to measure cell invasion and migration. Transfected glioma cells were suspended in the upper chamber in serum-free media of the Transwell. Then, 10% FBS was added to the medium in the lower chamber of the Transwell. After an incubation period, cells with moving cell membranes were stained with DAPI and fixed with 4% paraformaldehyde. Lastly, the quantity of migrating cells in the field of view was counted using inverted microscopy. The upper chamber was coated with Matrigel (BD Biosciences) for the cell invasion experiments, which were conducted as previously reported(19).

Flow cytometry

Glioma cells were separated using trypsin-EDTA (Life Technologies Inc., Beijing, China) and then cleaned with phosphate-buffered saline (PBS) for flow cytometry analysis. As directed by the manufacturer, stain cells with Annexin V and propidium iodide (PI) to distinguish between live, apoptotic, and necrotic cells. A flow cytometer (Jiyuan, Guangzhou, China) was used to conduct the flow cytometry. To calculate the apoptosis rate, data were examined using FlowJo software (FlowJo, Hangzhou, China). To evaluate cell cycle distribution, cells were fixed in 70% ethanol for an entire night at -20°C. They were then cleaned with PBS and stained with PI/RNase staining solution. Then, flow cytometry was employed to ascertain the cell distribution in the G1, S, and G2 phases. The results were plotted, and the proportion of cells in each cell cycle stage was assessed and compared under different experimental conditions to evaluate the effect of treatments on cell cycle progression.

12/15-HETE assay

Enzyme-linked immunosorbent assay (ELISA) kits specific for each chemical (12-HETE ELISA kits, ab133034, Abcam; 15-HETE ELISA kits, ab133035, Abcam) were used to measure the levels of 12-HETE and 15-HETE, in accordance with the procedures specified by the manufacturer. There were control, blank, standard, and sample wells on each 96-well plate, and each sample was analyzed twice. Initially, 50 µl of assay buffer and 100 µl of the suitable diluent were applied to the B0 (0 pg/ml standard) and non-specific binding (NSB) wells, respectively. All the wells were then filled with 50 µl of the 12/15-HETE alkaline phosphatase conjugate, and then the corresponding wells were filled with 50 µl of the 12/15-HETE antibody. The plates were incubated on a shaker at room temperature for 2 hours. The wells were cleaned three times using the supplied wash buffer following incubation. 200 µl of pNpp substrate solution and 5 µl of 12/15-HETE alkaline phosphatase conjugate were then added to each well. After that, the plates were incubated for three hours at 3°C without being shaken. A microplate reader (Molecular Devices, LLC) was used to measure the absorbance at 405 nm after the processes were stopped by adding 50 µl of stop solution to each well. To find the expression of 12/15-HETE, the mean net absorbance for each well was computed using the given formula.

Lactate dehydrogenase (LDH) assay

In accordance with the manufacturer's instructions, the LDH release was measured using a colorimetric CytoTox 96 Cytotoxicity kit (Promega Corporation). By subjecting the cultures to a 10× lysis solution, the maximum levels of LDH release were ascertained by measuring the entire lysis. A 96-well plate reader (Molecular Devices, LLC) was used to detect absorbance at 490 nm. LDH expression was calculated as a percentage by dividing experimental LDH release by maximal LDH release.

Statistical analysis

The statistical study was completed with the R program. Every experiment was conducted in triplicate, and the results were reported as mean ± standard deviation (SD).

Tukey's test was utilized for post-hoc analysis after one-way analysis of variance (ANOVA) was utilized to determine the significance of differences between groups. A $p< 0.05$ was considered statistically significant.

Results

Identification of DEGs in glioma samples

Using the R package, 1867 downregulated and 1255 upregulated DEGs were found from glioma samples and normal controls in the TCGA dataset. Additionally, 467 upregulated and 810 downregulated DEGs were screened from the GSE12657 dataset, while 1264 upregulated and 1346 downregulated DEGs were identified from the GSE16011 dataset. Furthermore, 10794 upregulated and 1814 downregulated DEGs were extracted from the GSE41031 dataset (Supplementary Figures 1A-1D). Subsequent intersection analysis revealed 137 overlapping upregulated DEGs and 178 overlapping downregulated DEGs across the four datasets (Supplementary Figures 1E and 1F).

PPI network and batch survival analysis of overlapping DEGs

PPI network analysis was performed on 315 overlapping DEGs using the Cytoscape software and STRING database. Three different gene module networks were generated according to the degree, MNC, and EPC algorithms (Supplementary Figures 2A-2C). Subsequent intersection analysis of DEGs within the three network modules identified 19 overlapping genes (Supplementary Figure 2D). Prognostic evaluation of OS for these 19 genes revealed significant prognostic value for 17 genes, as shown in the forest plot (Supplementary Figure 2E).

Identification and prognostic assessment of 13 characteristic genes of glioma

Through LASSO Cox regression analysis, 13 prognostic genes were identified with the optimal lambda value (lambda.min=0.005) (Supplementary Figures 3A and 3B). The risk scores for these genes were determined as follows: Riskscore=(0.0041)**NPY*+(0.2462)**CALM3*+(0.2346)**CDK4*+(-0.551)**VAMP2*+(0.0687)**SYT1*+(0.0426)**EGFR*+(0.072)**ANK3*+(0.0661)**CCK*+(-0.2637)**SCN2A*+(0.1766)**CALM1*+(-0.3069)**STXBP1*+(0.1075)**SNAP25*+(0.3827)**FN1*. In risk model analysis, in comparison to the low-risk group, the high-risk group showed lower survival rates and greater death rates (Supplementary Figures 3C). KM survival analysis results depicted a median survival time of 2 years for the high-risk group and 9.5 years for the low-risk group, with an HR of 4.666 (>1) (Supplementary Figure 3D). Additionally, the high-risk group had a reduced OS probability. ROC curve results further emphasized the predictive accuracy of the risk model, particularly at 3 years (AUC=0.856) (Supplementary Figure 3E). In summary, our study underscores the significant prognostic potential of these 13 genes.

Identification of hub genes in glioma risk model analysis

Key genes and clinical factors (age, grade stage) in gliomas were assessed for their

predictive value using univariate and multivariate Cox regression models. Four significant prognostic factors were identified, including *CDK4*, *STXBP1*, *VAMP2*, and age (Figures 1A and 1B). Nomogram analysis revealed their significant capacity for prediction for patients' 1-year, 3-year, and 5-year survival rates, corroborated by calibration curve results (Figures 1C and 1D). Expression analysis indicated significant upregulation of *CDK4* and downregulation of *STXBP1* and VAMP2 in tumor samples across TCGA-glioma, GSE12657, GSE16011, and GSE41031 datasets (Figures 1E-1H). A study has demonstrated that *STXBP1* is associated with the prognosis of GBM. Therefore, *STXBP1* was chosen as a hub gene for further investigation in this research due to its prognostic significance and differential expression.

Knockdown of *STXBP1* enhances the proliferation, migration, and invasion abilities of U251 and U87 cells

To assess the role of *STXBP1* in glioma, we assessed its level in glioma cell lines and HEB cells. qRT-PCR analysis revealed significantly lower *STXBP1* mRNA levels in glioma cell lines (U251, SW1783, and U87) in contrast to HEB cells (Figure 2A). WB analysis confirmed reduced STXBP1 protein levels in these glioma cell lines (Figures 2B and 2C). We then performed knockdown experiments using three different siRNAs targeting *STXBP1* (si-*STXBP1*-1, si-*STXBP1*-2, and si-*STXBP1*-3) in U87 and U251 cells. It was subsequently proven that si-*STXBP1*-1 and si-*STXBP1*-2 had significant knockout efficiency, among which si-*STXBP1*-1 showed the highest knockout efficiency and was selected for further experiments (Figures 2D-2F). Functional assays including CCK-8 and transwell assays indicated that si-*STXBP1*-1 induced increased invasion, migration, and proliferation capabilities in U251 and U87 cells (Figures 2G-2L).

Knockdown of *STXBP1* disrupts cell cycle distribution and inhibits apoptosis in glioma cells

Flow cytometry analysis was performed to assess the effect of *STXBP1* knockdown on cell cycle distribution in U251 and U87 glioma cells. Knockdown of *STXBP1* led to a significant rise in the percentage of G1 phase cells and a comparable decline in the S phase compared to control cells (si-NC) in both U251 and U87 cells (Figures 3A-3D). WB analysis assessed the expression of cell cycle-related proteins Cyclin B1, CDK1, and Cyclin A2. The findings demonstrated that STXBP1 knockdown notably upregulated the levels of these proteins in both U87 and U251 cells (Figures 3E-3G). Additionally, flow cytometry was employed to measure apoptosis rates in U87 and U251 cells following *STXBP1* knockdown. The results indicated a significant decrease in apoptosis rates in *STXBP1* knockdown cells in contrast to control cells (Figures 3H-3I).

Ferroptosis markers were significantly expressed in U251 and U87 cells

The levels of *GPX4*, a key regulator of ferroptosis, were assessed in glioma cell lines (SW1783, U251, and U87) and human embryonic brain (HEB) cells. qRT-PCR analysis revealed significantly higher *GPX4* mRNA levels in glioma cell lines compared to HEB

cells (Figure 4A). WB analysis confirmed the upregulation of GPX4 protein in glioma cell lines (Figures 4B and 4C). Additionally, the levels of 12-HETE and 15-HETE, markers of lipid peroxidation, were measured in glioma cell lines and HEB cells utilizing 12/15 HETE ELISA kits (ab133034/ab133035, Abcam). The results indicated significantly lower levels of 15-HETE and 12-HETE in glioma cell lines compared to HEB cells (Figures 4D and 4E).

Effects of ferroptosis inducers and inhibitors on LDH release and cell viability in glioma cells

To investigate the results of inhibitors and inducers of ferroptosis on glioma cells, we assessed LDH release and cell viability in U251 and U87 cell lines. Therapy with ferroptosis inducers (5 μM Sorafenib and 10 μM erastin) significantly increased LDH release in both U251 and U87 cells compared to the control (Figure 5A). Conversely, application of ferroptosis inhibitors (1 μM ferrostatin-1 and 5 μM U0126) led to a reduction of LDH release compared to the DMSO control (Figure 5B). Using the CCK-8 assay to assess cell viability, the administration of ferroptosis inducers (5 μM Sorafenib and 10 μM erastin) significantly decreased cell viability in both U251 and U87 cells compared to the control (Figures 5C and 5D). In contrast, use of ferroptosis inhibitors (1 μM ferrostatin-1 and 5 μM U0126) significantly increased cell viability over the same period (Figures 5E and 5F). These findings suggest that inducers of ferroptosis promote cytotoxicity and reduce cell viability in glioma cells, while ferroptosis inhibitors have the opposite effect, highlighting the potential medicinal uses of ferroptosis in glioma treatment.

Knockdown of *STXBP1* inhibits ferroptosis in glioma cells to reduce proliferation

To explore the impact of *STXBP1* knockdown on lipid peroxidation and cell viability, we measured the expression of 12-HETE and 15-HETE, LDH release, and cell viability in glioma cell lines. Knockdown of *STXBP1* significantly reduced the expression of both 15-HETE and 12-HETE compared to the control group (Figures 6A and 6B). LDH release assays revealed that *STXBP1* knockdown significantly reduced LDH release in both U251 and U87 cells, indicating enhanced cell damage. However, when combined with Sorafenib treatment, *STXBP1* knockdown partially rescued the LDH release induced by Sorafenib in both U251 and U87 cells (Figures 6C and 6D). CCK-8 assay showed that knockdown of *STXBP1* increased cell viability compared with the control group. Furthermore, *STXBP1* knockdown notably attenuated the sorafenib-induced reduction in cell viability in U251 and U87 cells when combined with sorafenib (Figures 6E and 6F). These results indicate that STXBP1 knockdown reduced 12-HETE and 15-HETE levels, suppressed lipid peroxidation, and inhibited ferroptosis, thereby enhancing glioma cell viability, highlighting its potential role in regulating ferroptosis and cell survival.

***STXBP1* regulates the EMT of ferroptosis-dependent tumor cells**

N-cadherin, Vimentin, and E-cadherin are proteins associated with EMT. qRT-PCR and WB analyses revealed that treatment with 1μM ferrostatin-1 induced a decrease in N-

cadherin and Vimentin levels and a significant increase in E-cadherin levels in glioma cells. Conversely, the addition of si-*STXBP1*-1 reversed these changes (Figures 7A-7E). Furthermore, CCK-8 and transwell assays demonstrated that treatment with 1μM ferrostatin-1 improved the viability, invasion, and migration capabilities of glioma cells, while the addition of si-*STXBP1*-1 further augmented these cellular functions (Figures 7F-7K). These results indicate that STXBP1 knockdown promotes EMT and enhances the aggressive behavior of glioma cells in a ferroptosis-dependent manner, suggesting its pivotal role in the development of gliomas and as a target for treatment.

Discussion

Gliomas are extremely aggressive brain tumors that have a dismal prognosis and few available treatments(20). These tumors, derived from glial cells, exhibit distinct histological and molecular characteristics. Despite advances in standard treatments such as chemotherapy, radiation therapy, and surgical resection, the survival rates for glioma individuals, particularly those with high-grade tumors, remain dismal(21). Therefore, developing novel treatment approaches requires a knowledge of the molecular processes underlying the growth of gliomas. For example, a study has found that Isoliquiritigenin can inhibit the tumorigenesis of glioma by suppressing circ0030018 via the miR-1236/HER2 signaling pathway, and circ0030018 can serve as a potential biomarker or therapeutic target for glioma(22). Yan et al. discovered that METTL3 promotes HNRNPH1-mediated selective splicing of LINC00475, thereby facilitating glioma progression through mitochondrial fission. Targeting the selective splicing of LINC00475 and m6A modification can be considered a therapeutic strategy against glioma(23). From the TCGA-glioma, GSE12657, GSE16011, and GSE41031 datasets, we identified upregulated and downregulated DEGs. Cross-analysis revealed overlapping DEGs, followed by PPI network analysis, OS prognosis assessment, advanced prognostic analysis, and expression analysis. Notably, *STXBP1* emerged as a hub gene. Previous studies by Zhen W et al. and Kajana X et al. corroborate our findings. Zhen W et al. highlighted the prognostic relevance of m7G-related genes in low-grade glioma (LGG), with particular emphasis on the association of *STXBP1* with macrophage M2 in LGG patients(24). Similarly, Kajana X et al. observed enriched *STXBP1* levels in extracellular vesicles (EVs) from the cerebrospinal fluid (CSF) of pediatric glioma patients, suggesting its potential as a malignancy marker and implicating its role in glioma pathogenesis and prognosis(25). These studies collectively support the pivotal role of *STXBP1* in glioma progression. In conclusion, our findings contribute to a deeper understanding of glioma biology and emphasize the significance of *STXBP1* as a potential therapeutic objective and prognostic indicator in glioma management.

Cell apoptosis, also known as programmed cell death, is a crucial mechanism that keeps tissues maintaining tissue homeostasis and getting rid of damaged or aberrant cells(26). It includes a series of biochemical processes leading to DNA fragmentation, chromatin condensation, cell shrinkage, and cell death(27). Proteins such as CDK-1, Cyclin B1, and Cyclin A2 are crucial regulators of the cell cycle and apoptosis. Aberrant expression

or activity of these proteins can influence apoptotic pathways, either promoting or inhibiting cell death depending on the cellular context and signaling pathways involved. For instance, Yang Y et al. found that Rab3a enhances neuronal cell-derived EV secretion by interacting with *STXBP1*, inhibiting M1 macrophage polarization, and reducing neuronal apoptosis, thus aiding spinal cord injury repair(28). Lv Y et al. observed increased DNA methylation in neurons during hypoxia, activating apoptotic signaling pathways(29). Hypermethylated *STXBP1* suggests its involvement in regulating neuronal death, suggesting that it might be employed as a therapeutic target for ischemia-reperfusion injury-induced neuronal damage. Bhawe K et al. demonstrated that high NRF1 activity in astrocytoma correlates with cancer aggressiveness and poor prognosis in GBM(30). Decreased *STXBP1* expression predicts GBM malignancy in high *NRF1* expression, underscoring the role of *STXBP1* in GBM progression and suggesting *NRF1* as a therapeutic target. Our findings align with these studies, revealing that knocking down *STXBP1* enhances the migration, proliferation, and invasion capabilities of glioma cells. Additionally, *STXBP1* knockdown disrupts glioma cell cycle distribution and inhibits apoptosis, highlighting its significant impact on glioma progression. Overall, these findings emphasize the multifaceted role of *STXBP1* in glioma biology, influencing cell cycle regulation, apoptosis, and cellular behaviors critical to tumor progression.

Ferroptosis is a controlled type of cellular demise typified by lipid peroxidation that is dependent on iron, leading to the aggregation of lipid hydroperoxides and subsequent cell membrane damage(31). Zuo Z et al. showed the prognostic significance of genes linked to ferroptosis signatures in glioma, employing a deep learning network trained with multiparametric MRI data(32). This study highlighted the potential for novel therapeutic strategies and prognosis assessment. Zhuo S et al. identified distinct expression profiles of ferroptosis-related genes in glioma, categorizing them into subgroups and developing a 25-gene risk signature correlated with clinical characteristics, serving as a prognostic signal(33). GPX4, a key enzyme in this process, detoxifies lipid hydroperoxides, defending against oxidative damage and stopping ferroptosis in cells(34). Additionally, the peroxidation of lipid products such as 12-HETE and 15-HETE is associated with ferroptosis, which contributes to oxidative stress and promotes cell membrane damage(35). LDH release is another critical marker, indicating cell membrane integrity and damage, which is often associated with cytotoxicity and cell death. Our findings indicate that ferroptosis inducers (erastin and Sorafenib) increase cytotoxicity in glioma cells, whereas the inhibitors of ferroptosis (U0126 and ferrostatin-1) provide a protective effect. Additionally, knocking down *STXBP1* in glioma cells inhibits ferroptosis, enhancing cell viability and mitigating cytotoxic effects. To sum up, our research demonstrates the critical function of ferroptosis regulation in glioma cell survival, with *STXBP1* playing a significant modulatory role. Targeting ferroptosis pathways and modulating *STXBP1* expression may offer novel therapeutic strategies for glioma treatment.

However, the use of ferroptosis activators can induce the release of LDH, which

indicates cell necrosis and can lead to inflammatory reactions, thereby affecting the survival of normal cells. To avoid necrosis and inflammation in normal cells when using ferroptosis activators, some current related studies include: (1) Targeted Delivery: Using antibody or nanoparticle conjugates to selectively deliver activators to cancer cells, thereby reducing systemic toxicity(36, 37). (2) Dual Inhibitors: As identified by the research team at Tongji University, compounds like KW-2449 can act as dual inhibitors of both ferroptosis and necroptosis. KW-2449 targets the autophagy pathway, specifically inhibiting ULK1 kinase activity, which in turn prevents ferroptosis. This suggests that by modulating autophagy, it may be possible to control ferroptosis in a way that minimizes damage to normal cells(38). (3) Temporal Control: Controlled-release manner to induce ferroptosis without overwhelming normal cells(39, 40). (4) Cell-Type Specific Modulators: Identifying and exploiting cell-type specific differences in the ferroptosis pathway could also be beneficial. For example, if certain enzymes or proteins involved in ferroptosis are differentially expressed in cancer cells compared to normal cells, then inhibitors or activators that target these specific components could be used to selectively induce ferroptosis in the cancer cells(40). In conclusion, while the use of ferroptosis activators holds great promise for cancer therapy, it is crucial to develop strategies that minimize their impact on normal cells. The approaches outlined above, based on current research findings, offer potential solutions to this challenge. Further research is needed to optimize these strategies and to better understand the complex interplay between ferroptosis, necrosis, and inflammation.

The biological process known as the epithelial-mesenchymal transition (EMT) occurs when epithelial cells shift molecularly to take on the characteristics of mesenchymal cells(41). This transition enables cells to acquire migratory and invasive properties. E-cadherin, a cell adhesion molecule, is downregulated during EMT, leading to loss of cell-cell adhesion(42). Conversely, N-cadherin, another adhesion molecule, is upregulated, promoting cell migration and invasion(43). Vimentin, an intermediate filament protein, increases during EMT, enhancing cell motility and cytoskeletal remodeling(44). Together, these changes facilitate the transformation of epithelial cells into a mesenchymal state, promoting tumor metastasis and progression. Zou S discovered that JMJD3 stimulates glioma cell migration by inducing EMT through the CXCL12/CXCR4 axis, highlighting its potential as a therapeutic target(45). Additionally, Zou M found that DYT-40 inhibits AEG-1 and NF-κB pathways, suppressing EMT and invasion in glioblastoma while inducing apoptosis via the mitochondrial pathway(46). Furthermore, another study by Zou M revealed that AEG-1-induced autophagy enhances glioma cell susceptibility to TGF-β1-induced EMT, promoting tumor progression(47). Inhibition of autophagy suppresses EMT, suggesting a complex interplay between AEG-1, autophagy, and EMT in glioblastoma progression. Our study found that 1 μM Ferrostatin-1 treatment induced a significant decrease in N-cadherin and Vimentin expression and an increase in E-cadherin expression in glioma cells. In contrast, the addition of si-*STXBP1*-1 reversed these changes. CCK-8 and transwell test results were the same. Treatment with 1 μM Ferrostatin-1 improved

glioma cells' viability, invasion, and migration capabilities, while adding si-*STXBP1*-1 further enhanced these cell functions. This highlights the potential therapeutic value of targeting EMT-related pathways and the ferroptosis regulator (*STXBP1*) in glioma treatment.

While our study provides valuable insights into the role of *STXBP1* in glioma progression through in vitro experiments and bioinformatics analysis, there are several limitations that need to be addressed. One significant limitation is the absence of in vivo tumor graft experiments. These experiments are crucial for validating the findings from in vitro studies and assessing the potential therapeutic effects of targeting *STXBP1* in a more physiologically relevant context. The lack of such experiments limits the extent to which we can extrapolate our findings to clinical settings. In future work, we plan to conduct in vivo tumor graft experiments using glioma cell lines with *STXBP1* knockdown to investigate the impact on tumor growth, invasion, and overall survival in animal models. These experiments will provide a more comprehensive understanding of the role of *STXBP1* in glioma progression and help validate its potential as a therapeutic target.

Conclusion

In conclusion, our study identified distinct DEGs associated with glioma progression and prognosis, highlighting their potential as prognostic indicators and therapeutic targets. Additionally, the identification and assessment of characteristic genes, including the hub gene *STXBP1*, provided valuable insights into glioma biology and progression. Knockdown of *STXBP1* significantly enhanced glioma cell invasion, migration, and proliferation, affecting apoptosis and cell cycle distribution. Furthermore, our findings elucidated the role of ferroptosis in glioma cell viability, with Sorafenib and erastin inducing ferroptosis and reducing cell viability, while ferrostatin-1 and U0126 inhibited ferroptosis and increased cell viability. Notably, the knockdown of *STXBP1* inhibited ferroptosis and regulated EMT-related proteins, further emphasizing its pivotal role in glioma progression. Overall, our study sheds light on the complex interplay between *STXBP1*, ferroptosis, and EMT in glioma pathogenesis, suggesting potential therapeutic strategies targeting these pathways for improved glioma treatment outcomes.

Authors' Contribution

Conception and design of the research: Xuemin Li and Chonggong Zhang
Acquisition of data: Xuemin Li , Chonggong Zhang and Peiyu Qian
Analysis and interpretation of data: Xuemin Li
Statistical analysis: Chonggong Zhang and Peiyu Qian
Drafting the manuscript: Xuemin Li and Chonggong Zhang
Revision of manuscript for important intellectual content: Xuemin Li and Chonggong Zhang

Ethics approval and consent to participate

Not applicable.

Consent for publication

Not applicable.

Availability of data and materials

The datasets used and/or analyzed during the current study are available from the corresponding author upon reasonable request.

Competing interests

The authors have no conflicts of interest to declare.

Funding

None.

Acknowledgments

None.

Figure legends

Figure 1. Identification of hub genes in glioma risk model analysis.

(A and B) Univariate/multifactorial Cox regression analysis on signature genes and clinical prognostic variables.

(C) Nomograms of key prognostic variables and C-index were used to evaluate the predictive power of the model.

(D) The dashed line indicates the ideal calibration curve of the nomogram with the red dash, purple dash, and yellow dash for the 1-year, 3-year, and 5-year predictions, respectively.

(E-H) The expression of prognostic significant genes *CDK4*, *STXBP1*, and VAMP2 in tumor samples and normal of TCGA-glioma, GSE12657, GSE16011, and GSE41031 datasets respectively. Among them, purple represents normal samples and red represents tumor samples.

TCGA, The Cancer Genome Atlas.

*p<0.05, **p<0.01, ***p<0.001, ****p<0.0001.

Figure 2. Knockdown of *STXBP1* enhances the proliferation, migration, and invasion abilities of U251 and U87 cells.

(A-C) qRT-PCR and WB detected the expression of *STXBP1* in normal brain glial cells (HEB) and brain glioma cells (U251, SW1783, and U87).

(D-F) *STXBP1* was knocked down, and the knockdown efficiency of si-*STXBP1*-1, si-*STXBP1*-2, and si-*STXBP1*-3 was detected by qRT-PCR and WB.

(G and H) CCK-8 detects the effect of si-*STXBP1*-1 on U251 and U87 cell viability.

(I-L) Transwell was used to detect the effect of si-*STXBP1*-1 on the migration and invasion abilities of U251, SW1783, and U87 cells.

qRT-PCR: Quantitative real-time polymerase chain reaction, WB: Western blot, CCK-8: Cell counting kit-8.
*p<0.05. Scale bar: 50m.

Figure 3. Effects of *STXBP1* knockdown on cell cycle progression and apoptosis in glioma cells.
(A-D) Flow cytometry was used to detect the effect of si-*STXBP1*-1 on the cell cycle of U251, SW1783, and U87.
(E-G) WB detected the effect of si-STXBP1-1 on cell cycle proteins in U251 and U87 cells. Cyclins include CDK-1, Cyclin B1, and Cyclin A2.
(H and I) Flow cytometry was used to detect the effect of knocking down *STXBP1* on the apoptosis of U251 and U87 cells.
WB: Western blot.
*p<0.05.

Figure 4. Expression of GPX4 and Levels of 12-HETE and 15-HETE in glioma cells.
(A) Relative expression levels of *GPX4* mRNA in human embryonic brain (HEB) cells and glioma cell lines (SW1783, U251, U87) as determined by qRT-PCR.
(B and C) WB analysis of GPX4 protein levels in HEB cells and glioma cell lines (SW1783, U251, U87).
(D) The 12-HETE kit detects 12-HETE levels in HEB cells and glioma cells (U251, SW1783 and U87).
(E) The 15-HETE kit detects 15-HETE levels in HEB cells and glioma cells (U251, SW1783 and U87).
qRT-PCR: Quantitative real-time polymerase chain reaction, WB: Western blot.
*p<0.05, **p<0.01

Figure 5. Effects of ferroptosis inducers and inhibitors on LDH release and cell viability in glioma cells.
(A) The LDH detection kit detects the LDH release level of glioma cells after treatment with the ferroptosis inducer sorafenib (5μM) or erastin (10μM).
(B) The LDH detection kit detects the LDH release level of glioma cells after treatment with ferroptosis inhibitor ferrostatin-1 (1μM) or U0126 (5μM).
(C and D) Cell viability of glioma cells treated with control, 5 μM DMSO, 5 μM Sorafenib, or 10 μM erastin.
(E and F) Cell viability of glioma cells treated with control, 5 μM DMSO, 1 μM ferrostatin-1, or 5 μM U0126.
LDH: lactate dehydrogenase, CCK-8: Cell counting kit-8.
*p<0.05.

Figure 6. Effects of *STXBP1* knockdown and ferroptosis induction on lipid peroxidation, LDH release, and cell viability in glioma cells.
(A and B) 12-HETE kit and 15-HETE kit detect expression in U251 and U87 cells after

knockdown of *STXBP1*.
(C and D) The LDH kit detects changes in LDH release in U251 and U87 cells. The groups are as follows: control; 5μM DMSO; si-NC; 5μM Sorafenib; si-*STXBP1*-1; 5μM Sorafenib+si-*STXBP1*-1.
(E and F) CCK-8 detects changes in glioma cell viability. The groups are as follows: control; 5μM DMSO; si-NC; 5μM Sorafenib; si-*STXBP1*-1; 5μM Sorafenib+si-*STXBP1*-1.
LDH: lactate dehydrogenase, CCK-8: Cell counting kit-8, si-NC: small interfering-negative control, DMSO: Dimethyl sulfoxide.
*p<0.05 vs. control or 5μM DMSO or si-NC, #p<0.05 vs. 5μM Sorafenib or si-*STXBP1*-1.

Figure 7. Effects of *STXBP1* knockdown and ferrostatin-1 treatment on EMT markers, cell viability, invasion, and migration of glioma cells.
(A and B) qRT-PCR detected the expression of EMT-related markers (*E-cadherin*, *N-cadherin*, and *Vimentin*) after knocking down *STXBP1* and combining ferroptosis inhibitor ferrostatin-1 (1μM) in glioma cells.
(C-E) WB detected the expression of EMT-related markers (E-cadherin, N-cadherin, and Vimentin) after knocking down STXBP1 and combining ferroptosis inhibitor ferrostatin-1 (1μM) in glioma cells.
(F and G) Cell viability of glioma cells treated with control, 1 μM ferrostatin-1, si-*STXBP1*-1, or a combination of si-*STXBP1*-1 and 1 μM ferrostatin-1.
(H-K) Transwell detects changes in the migration and invasion ability of glioma cells. The groups are as follows: control; 1μM ferrostatin-1; si-*STXBP1*-1; 1μM ferrostatin-1+si-*STXBP1*-1.
qRT-PCR: Quantitative real-time polymerase chain reaction, WB: Western blot, CCK-8: Cell counting kit-8.
*p<0.05 vs. control, #p<0.05 vs. si-*STXBP1*-1 or 1μM ferrostatin-1.

Supplementary Figure 1. Identification of DEGs in glioma samples.
(A-D) DEGs screening of TCGA-glioma dataset (A), GSE12657 dataset (B), GSE16011 dataset (C), and GSE41031 dataset (D). Red represents up-regulated DEGs, and purple represents down-regulated DEGs.
(E and F) Cross-analysis was performed on the up-regulated DEGs and down-regulated DEGs of the TCGA-glioma data set, GSE12657 data set, GSE16011 data set, and GSE41031 data set, respectively.
DEGs: Differentially expressed genes; TCGA, The Cancer Genome Atlas.

Supplementary Figure 2. PPI network and batch survival analysis of overlapping DEGs.
(A-C) PPI network analysis of overlapping DEGs, including degree, MNC, and EPC. Nodes represent proteins or protein domains, while edges represent interactions between these proteins.
(D) Venn diagram, intersection analysis of DEGs in three network modules, with the

overlapping genes in the middle.
(E) Forest plot of the OS prognostic value of the 17 overlapping genes.
PPI: Protein-Protein Interaction, MNC: Maximum Neighborhood Component, EPC: Edge Percolated Component, DEGs: Differentially expressed genes, OS: overall survival.

Supplementary Figure 3. Identification and prognostic assessment of 13 characteristic genes of glioma.
(A) LASSO-Cox regression model analysis of significant genes for OS prognosis.
(B) The relationship between 10-fold cross-validation partial likelihood deviation and log(λ).
(C) Risk model analysis of the selected sample data, the upper panel shows the risk samples, the middle panel shows the survival status, and the lower panel shows the heatmap of the clustering distribution of signature genes.
(D) The KM survival curve analysis of the two groups in the risk model, the red line indicates the high-risk group and the blue line indicates the low-risk group.
(E) ROC curve analysis on the risk model in patients at 1, 3, and 5 years, the horizontal coordinate is a false positive fraction, and the vertical coordinate is a true positive fraction.
LASSO: Least Absolute Shrinkage and Selection Operator, KM: Kaplan-Meier, ROC: Receiver Operating Characteristic.

Table 1. Primer sequences for qRT-PCR.

Target	Direction	Sequence (5'-3')
STXBP1	Forward	GGGTATGGAACGGTAGAAA
STXBP1	Reverse	GTAGGGACTGGAATGAAGATAG
GPX4	Forward	GAGGCAAGACCGAAGTAAACTAC
GPX4	Reverse	CCGAACTGGTTACACGGGAA
E-cadherin	Forward	CGCATTGCCACATACACTCT
E-cadherin	Reverse	TTGGCTGAGGATGGTGTAAG
N-cadherin	Forward	AGTCAACTGCAACCGTGTGT
N-cadherin	Reverse	AGCGTTCCTGTTCCACTCAT
Vimentin	Forward	CAGGAGGCAGAAGAATGGTACAAA
Vimentin	Reverse	GGCGTTCCAGGGACTCATTG
GAPDH	Forward	CTCGCTTCGGCAGCACATATACT
GAPDH	Reverse	ACGCTTCACGAATTTGCGTGTC

References

1. Smith HL, Wadhwani N, Horbinski C. Major features of the 2021 WHO classification of CNS tumors. Neurotherapeutics. 2022;19(6):1691-704.
2. Pienkowski T, Kowalczyk T, Kretowski A, Ciborowski M. A review of gliomas-related proteins. Characteristics of potential biomarkers. American Journal of Cancer Research. 2021;11(7):3425.
3. Nandihal P, Shetty V, Guha T, Pareek PK, editors. Glioma Detection using Improved

Artificial Neural Network in MRI Images. 2022 IEEE 2nd Mysore Sub Section International Conference (MysuruCon); 2022: IEEE.
4. Yoda RA, Cimino PJ, editors. Classification and Grading of Central Nervous System Tumors According to the World Health Organization 5th Edition. Seminars in Neurology; 2023: Thieme Medical Publishers, Inc.
5. Weller M, Wen PY, Chang SM, Dirven L, Lim M, Monje M, et al. Glioma. Nature reviews Disease primers. 2024;10(1):33.
6. Sharma A, Graber JJ. Overview of prognostic factors in adult gliomas. Annals of palliative medicine. 2021;10(1):86374-874.
7. Jiang T, Nam D-H, Ram Z, Poon W-s, Wang J, Boldbaatar D, et al. Clinical practice guidelines for the management of adult diffuse gliomas. Cancer letters. 2021;499:60-72.
8. Śledzińska P, Bebyn MG, Furtak J, Kowalewski J, Lewandowska MA. Prognostic and predictive biomarkers in gliomas. International journal of molecular sciences. 2021;22(19):10373.
9. Freibauer A, Wohlleben M, Boelman C. STXBP1-Related Disorders: Clinical Presentation, Molecular Function, Treatment, and Future Directions. Genes. 2023;14(12):2179.
10. Luo Y, Tian G, Fang X, Bai S, Yuan G, Pan Y. Ferroptosis and its potential role in glioma: from molecular mechanisms to therapeutic opportunities. Antioxidants. 2022;11(11):2123.
11. Zhu M, Wu P, Li Y, Zhang L, Zong Y, Wan M. Synergistic therapy for orthotopic gliomas via biomimetic nanosonosensitizer-mediated sonodynamic therapy and ferroptosis. Biomaterials Science. 2022;10(14):3911-23.
12. Zhou L, Jiang Z, Shi Z, Zhao W, Lu Z, Xie Y, et al. New Autophagy-Ferroptosis Gene Signature Predicts Survival in Glioma. Frontiers in Cell and Developmental Biology. 2021;9:739097.
13. Zheng Y, Ji Q, Xie L, Wang C, Yu CN, Wang YL, et al. Ferroptosis‐related gene signature as a prognostic marker for lower‐grade gliomas. Journal of cellular and molecular medicine. 2021;25(6):3080-90.
14. Zhou Y, Qian W, Li X, Wei W. NF-κB inhibitor myrislignan induces ferroptosis of glioblastoma cells via regulating epithelial-mesenchymal transformation in a slug-dependent manner. Oxidative Medicine and Cellular Longevity. 2023;2023.
15. Abramov D, Guiberson NGL, Burré J. STXBP1 encephalopathies: clinical spectrum, disease mechanisms, and therapeutic strategies. Journal of neurochemistry. 2021;157(2):165-78.
16. Zhang Y, Wang R, Liu Z, Jiang S, Du L, Qiu K, et al. Distinct genetic patterns of shared and unique genes across four neurodevelopmental disorders. American Journal of Medical Genetics Part B: Neuropsychiatric Genetics. 2021;186(1):3-15.
17. Zhou P, He N, Zhang JW, Lin ZJ, Wang J, Yan LM, et al. Novel mutations and phenotypes of epilepsy‐associated genes in epileptic encephalopathies. Genes, Brain and Behavior. 2018;17(8):e12456.
18. Stamberger H, Nikanorova M, Willemsen MH, Accorsi P, Angriman M, Baier H, et al. STXBP1 encephalopathy: a neurodevelopmental disorder including epilepsy. Neurology.

2016;86(10):954-62.
19. Aslan M, Hsu E-C, Liu S, Stoyanova T. Quantifying the invasion and migration ability of cancer cells with a 3D Matrigel drop invasion assay. Biology Methods and Protocols. 2021;6(1):bpab014.
20. Markouli M, Papachristou A, Politis A, Boviatsis E, Piperi C. Emerging Role of the Slit/Roundabout (Robo) Signaling Pathway in Glioma Pathogenesis and Potential Therapeutic Options. Biomolecules. 2024;14(10).
21. Wang LM, Englander ZK, Miller ML, Bruce JN. Malignant glioma. Human Brain and Spinal Cord Tumors: From Bench to Bedside Volume 2: The Path to Bedside Management: Springer; 2023. p. 1-30.
22. Liu A, Jiang B, Song C, Zhong Q, Mo Y, Yang R, et al. Isoliquiritigenin inhibits circ0030018 to suppress glioma tumorigenesis via the miR-1236/HER2 signaling pathway. MedComm. 2023;4(3):e282.
23. Yan Y, Luo A, Liu S, Cai M, Liu X, Zhang X, et al. METTL3-Mediated LINC00475 Alternative Splicing Promotes Glioma Progression by Inducing Mitochondrial Fission. Research (Washington, DC). 2024;7:0324.
24. Zhen W, Shan X, Cui X, Ji P, Zhang P, Wang M, et al. Exploration and validation of m7G-related genes as signatures in the immune microenvironment and prognostic indicators in low-grade glioma. American Journal of Translational Research. 2023;15(6):3882.
25. Kajana X, Spinelli S, Garbarino A, Balagura G, Bartolucci M, Petretto A, et al. Identification of Central Nervous System Oncologic Disease Biomarkers in EVs from Cerebrospinal Fluid (CSF) of Pediatric Patients: A Pilot Neuro-Proteomic Study. Biomolecules. 2023;13(12):1730.
26. Bedoui S, Herold MJ, Strasser A. Emerging connectivity of programmed cell death pathways and its physiological implications. Nature reviews Molecular cell biology. 2020;21(11):678-95.
27. Obeng E. Apoptosis (programmed cell death) and its signals-A review. Brazilian Journal of Biology. 2020;81:1133-43.
28. Yang Y, Liu Z, Lu Y, Yu X, Zhu R, Cai X, et al. Rab3a attenuates spinal cord injury by mediating vesicle release. Brain Research Bulletin. 2024;208:110884.
29. Lv Y, Zhang C, Jian H, Lou Y, Kang Y, Deng W, et al. Regulating DNA methylation could reduce neuronal ischemia response and apoptosis after ischemia-reperfusion injury. Gene. 2022;837:146689.
30. Bhawe K, Felty Q, Yoo C, Ehtesham NZ, Hasnain SE, Singh VP, et al. Nuclear respiratory factor 1 (NRF1) transcriptional activity-driven gene signature association with severity of astrocytoma and poor prognosis of glioblastoma. Molecular neurobiology. 2020;57:3827-45.
31. Wang L, Fang X, Ling B, Wang F, Xia Y, Zhang W, et al. Research progress on ferroptosis in the pathogenesis and treatment of neurodegenerative diseases. Frontiers in Cellular Neuroscience. 2024;18:1359453.
32. Zuo Z, Liu W, Zeng Y, Fan X, Li L, Chen J, et al. Multiparametric magnetic resonance imaging-derived deep learning network to determine ferroptosis-related gene signatures in gliomas. Frontiers in Neuroscience. 2022;16:1082867.

33. Zhuo S, Chen Z, Yang Y, Zhang J, Tang J, Yang K. Clinical and biological significances of a ferroptosis-related gene signature in glioma. Frontiers in oncology. 2020;10:590861.
34. Liu J, Kang R, Tang D. Signaling pathways and defense mechanisms of ferroptosis. The FEBS journal. 2022;289(22):7038-50.
35. Kuang F, Liu J, Tang D, Kang R. Oxidative damage and antioxidant defense in ferroptosis. Frontiers in cell and developmental biology. 2020;8:586578.
36. Li B, Chen X, Qiu W, Zhao R, Duan J, Zhang S, et al. Synchronous Disintegration of Ferroptosis Defense Axis via Engineered Exosome-Conjugated Magnetic Nanoparticles for Glioblastoma Therapy. Advanced science (Weinheim, Baden-Wurttemberg, Germany). 2022;9(17):e2105451.
37. Zhao Y, Fei Y, Zhao Y, Li M, Hu Y, Cai K, et al. Biomineralization-Tuned Nanounits Reprogram the Signal Transducer and Activator of Transcription 3 Signaling for Ferroptosis-Immunotherapy in Cancer Stem Cells. ACS nano. 2024;18(32):21268-87.
38. Zhao Y, Wang Q, Zhu J, Cai J, Feng X, Song Q, et al. Identification of KW-2449 as a dual inhibitor of ferroptosis and necroptosis reveals that autophagy is a targetable pathway for necroptosis inhibitors to prevent ferroptosis. Cell death & disease. 2024;15(10):764.
39. Han L, Peng K, Qiu LY, Li M, Ruan JH, He LL, et al. Hitchhiking on Controlled-Release Drug Delivery Systems: Opportunities and Challenges for Cancer Vaccines. Frontiers in pharmacology. 2021;12:679602.
40. Zhi Chen B, Ting He Y, Qiang Zhao Z, Hao Feng Y, Liang L, Peng J, et al. Strategies to develop polymeric microneedles for controlled drug release. Advanced drug delivery reviews. 2023:115109.
41. Navas T, Kinders RJ, Lawrence SM, Ferry-Galow KV, Borgel S, Hollingshead MG, et al. Clinical evolution of epithelial–mesenchymal transition in human carcinomas. Cancer research. 2020;80(2):304-18.
42. Santarosa M, Maestro R. The autophagic route of e-cadherin and cell adhesion molecules in cancer progression. Cancers. 2021;13(24):6328.
43. Choi S, Yu J, Kim W, Park K-S. N-cadherin mediates the migration of bone marrow-derived mesenchymal stem cells toward breast tumor cells. Theranostics. 2021;11(14):6786.
44. Usman S, Waseem NH, Nguyen TKN, Mohsin S, Jamal A, Teh M-T, et al. Vimentin is at the heart of epithelial mesenchymal transition (EMT) mediated metastasis. Cancers. 2021;13(19):4985.
45. Zou S, Zhang D, Xu Z, Wen X, Zhang Y. JMJD3 promotes the epithelial-mesenchymal transition and migration of glioma cells via the CXCL12/CXCR4 axis. Oncology Letters. 2019;18(6):5930-40.
46. Zou M, Duan Y, Wang P, Gao R, Chen X, Ou Y, et al. DYT-40, a novel synthetic 2-styryl-5-nitroimidazole derivative, blocks malignant glioblastoma growth and invasion by inhibiting AEG-1 and NF-κB signaling pathways. Scientific Reports. 2016;6(1):27331.
47. Zou M, Zhu W, Wang L, Shi L, Gao R, Ou Y, et al. AEG-1/MTDH-activated autophagy enhances human malignant glioma susceptibility to TGF-β1-triggered epithelial-

912 mesenchymal transition. Oncotarget. 2016;7(11):13122.
913

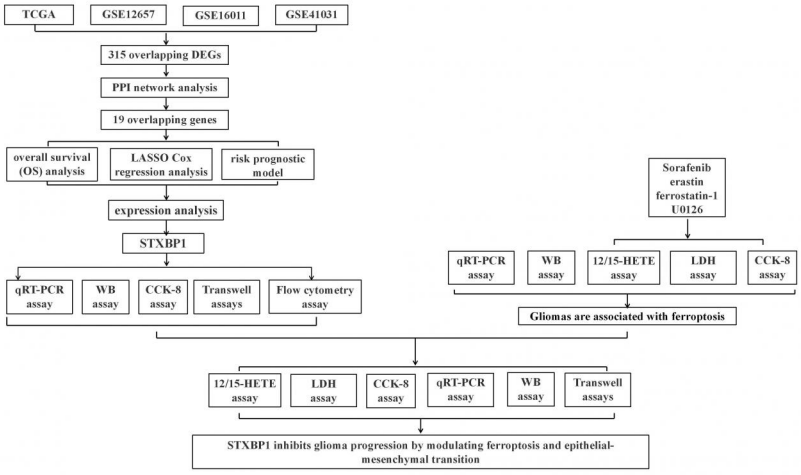

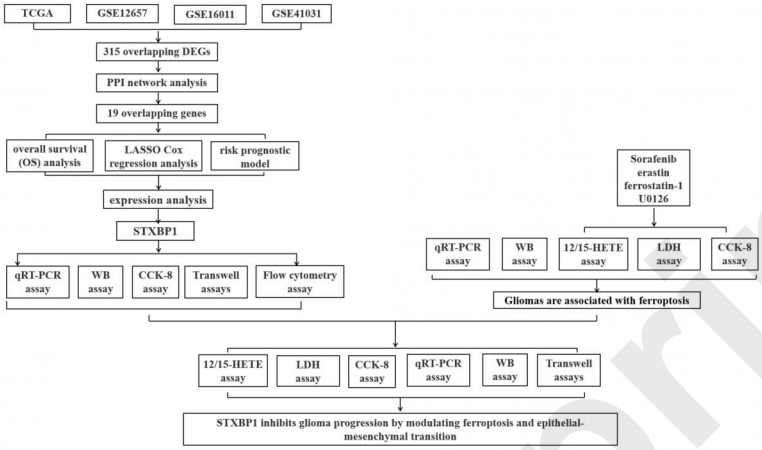

Differential gene expression analysis was performed on a glioma dataset, and protein-protein interaction (PPI) network analysis identified genes with significant prognostic value. Least absolute shrinkage and selection operator (LASSO) Cox regression analysis further narrowed the scope. Key genes were obtained through nomogram analysis, and expression verification was performed. In in vitro cell experiments, knockdown of STXBP1 was performed in glioma cell lines. The effects on cell proliferation, migration, invasion, cell cycle distribution, apoptosis, and markers of ferroptosis and EMT were assessed. After bioinformatics analysis, STXBP1 was identified as a hub gene. STXBP1 functions as a tumor suppressor in glioma, regulating ferroptosis and EMT. It presents potential as a therapeutic target in glioma management.

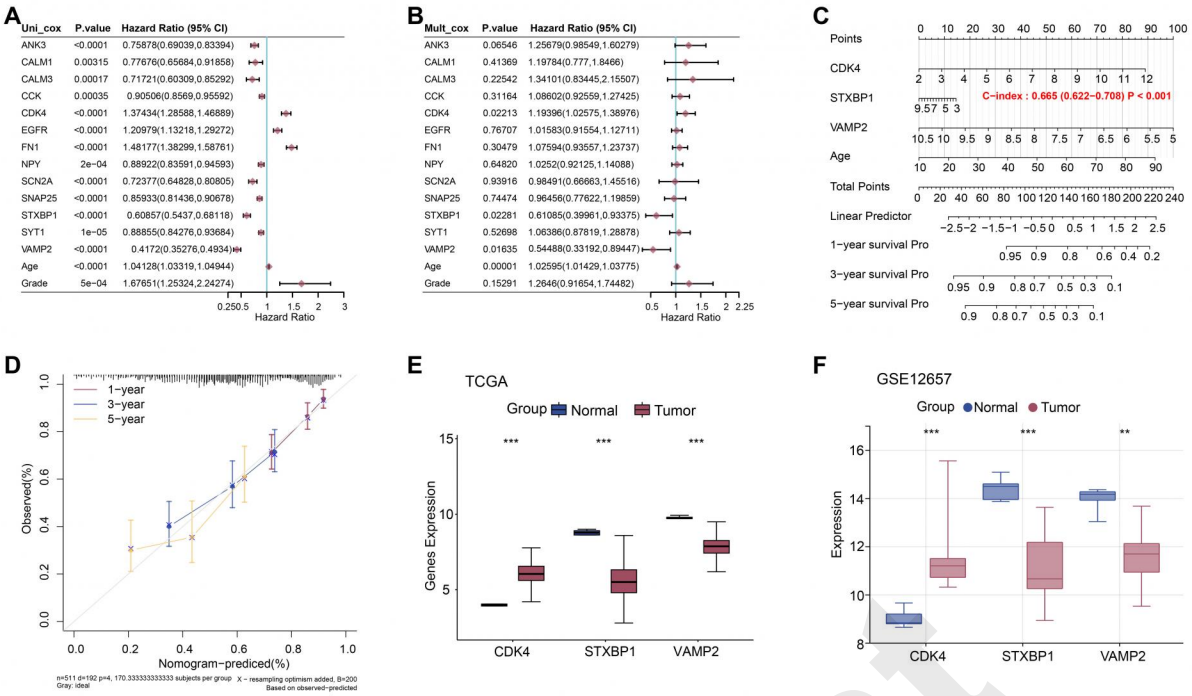
A
Uni_cox P.value Hazard Ratio (95% CI)
ANK3 <0.0001 0.75878(0.69039,0.83394)
CALM1 0.00315 0.77676(0.65684,0.91858)
CALM3 0.00017 0.71721(0.60309,0.85292)
CCK 0.00035 0.90506(0.8569,0.95592)
CDK4 <0.0001 1.37434(1.28588,1.46889)
EGFR <0.0001 1.20979(1.13218,1.29272)
FN1 <0.0001 1.48177(1.38299,1.58761)
NPY 2e-04 0.88922(0.83591,0.94593)
SCN2A <0.0001 0.72377(0.64828,0.80805)
SNAP25 <0.0001 0.85933(0.81436,0.90678)
STXBP1 <0.0001 0.60857(0.5437,0.68118)
SYT1 1e-05 0.88855(0.84276,0.93684)
VAMP2 <0.0001 0.4172(0.35276,0.4934)
Age <0.0001 1.04128(1.03319,1.04944)
Grade 5e-04 1.67651(1.25324,2.24274)
0.25 0.5 1 1.5 2 3
Hazard Ratio
B
Mult_cox P.value Hazard Ratio (95% CI)
ANK3 0.06546 1.25679(0.98549,1.60279)
CALM1 0.41369 1.19784(0.777,1.8466)
CALM3 0.22542 1.34101(0.83445,2.15507)
CCK 0.31164 1.08602(0.92559,1.27425)
CDK4 0.02213 1.19396(1.02575,1.38976)
EGFR 0.76707 1.01583(0.91554,1.12711)
FN1 0.30479 1.07594(0.93557,1.23737)
NPY 0.64820 1.0252(0.92125,1.14088)
SCN2A 0.93916 0.98491(0.66663,1.45516)
SNAP25 0.74474 0.96456(0.77622,1.19859)
STXBP1 0.02281 0.61085(0.39961,0.93375)
SYT1 0.52698 1.06386(0.87819,1.28878)
VAMP2 0.01635 0.54488(0.33192,0.89447)
Age 0.00001 1.02595(1.01429,1.03775)
Grade 0.15291 1.2646(0.91654,1.74482)
0.5 1 1.5 2 2.25
Hazard Ratio
C
Points
CDK4
STXBP1
VAMP2
Age
Total Points
Linear Predictor
1−year survival Pro
3−year survival Pro
5−year survival Pro
C−index : 0.665 (0.622−0.708) P < 0.001
D
1−year
3−year
5−year
Observed(%)
Nomogram−prediced(%)
E
TCGA
Group Normal Tumor
Genes Expression
CDK4 STXBP1 VAMP2
F
GSE12657
Group Normal Tumor
Expression
CDK4 STXBP1 VAMP2
G
GSE16011
Group Normal Tumor
Expression
CDK4 STXBP1 VAMP2
H
GSE41031
Group Normal Tumor
Expression
CDK4 STXBP1 VAMP2

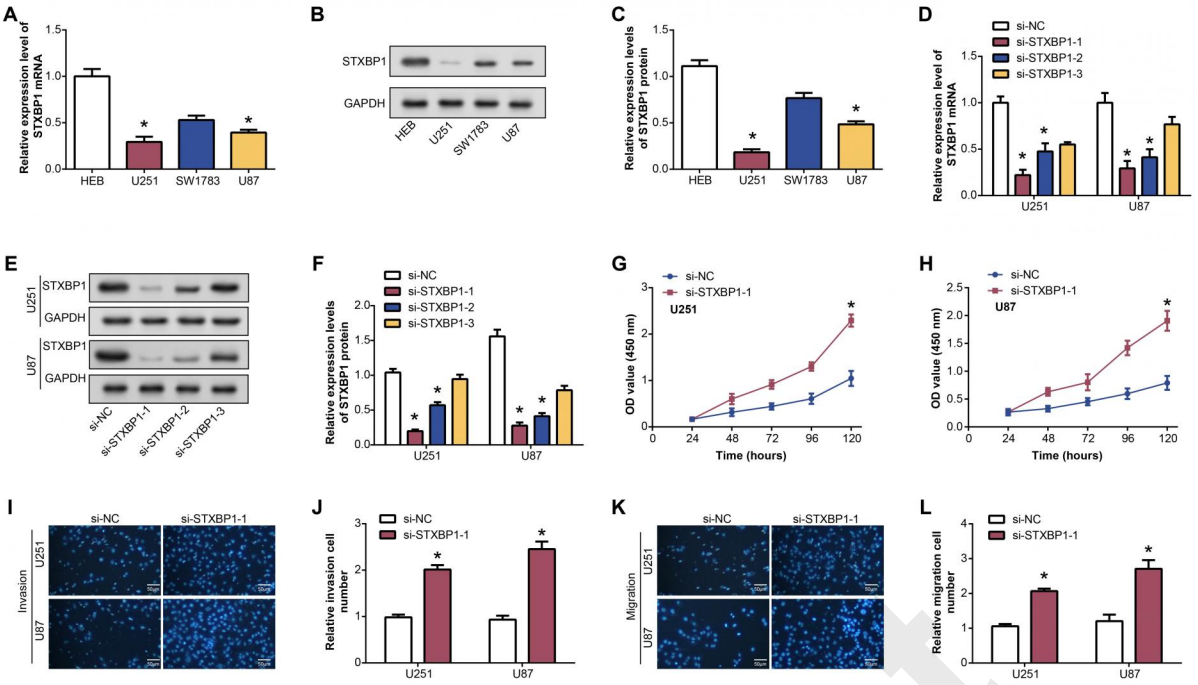
A
Relative expression level of STXBP1 mRNA
HEB
U251
SW1783
U87
B
STXBP1
GAPDH
HEB
U251
SW1783
U87
C
Relative expression levels of STXBP1 protein
HEB
U251
SW1783
U87
D
si-NC
si-STXBP1-1
si-STXBP1-2
si-STXBP1-3
Relative expression level of STXBP1 mRNA
U251
U87
E
U251
STXBP1
GAPDH
U87
STXBP1
GAPDH
si-NC
si-STXBP1-1
si-STXBP1-2
si-STXBP1-3
F
si-NC
si-STXBP1-1
si-STXBP1-2
si-STXBP1-3
Relative expression levels of STXBP1 protein
U251
U87
G
si-NC
si-STXBP1-1
U251
OD value (450 nm)
Time (hours)
H
si-NC
si-STXBP1-1
U87
OD value (450 nm)
Time (hours)
I
si-NC
si-STXBP1-1
Invasion
U251
U87
J
si-NC
si-STXBP1-1
Relative invasion cell number
U251
U87
K
si-NC
si-STXBP1-1
Migration
U251
U87
L
si-NC
si-STXBP1-1
Relative migration cell number
U251
U87

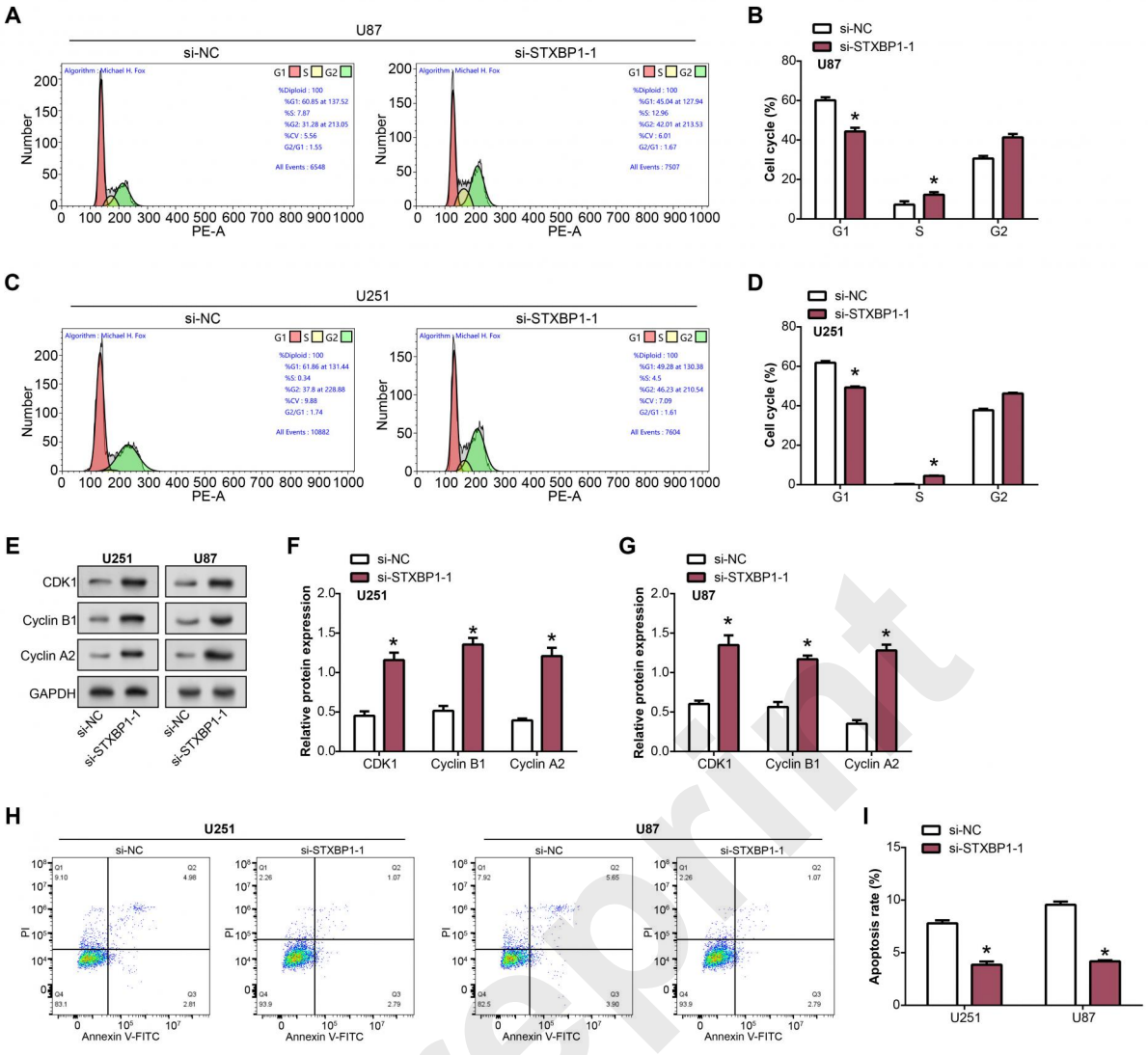
A
U87
si-NC
si-STXBP1-1
Number
PE-A
B
si-NC
si-STXBP1-1
U87
Cell cycle (%)
G1
S
G2
C
U251
si-NC
si-STXBP1-1
Number
PE-A
D
si-NC
si-STXBP1-1
U251
Cell cycle (%)
G1
S
G2
E
U251
U87
CDK1
Cyclin B1
Cyclin A2
GAPDH
si-NC
si-STXBP1-1
si-NC
si-STXBP1-1
F
si-NC
si-STXBP1-1
U251
Relative protein expression
CDK1
Cyclin B1
Cyclin A2
G
si-NC
si-STXBP1-1
U87
Relative protein expression
CDK1
Cyclin B1
Cyclin A2
H
U251
U87
si-NC
si-STXBP1-1
si-NC
si-STXBP1-1
PI
Annexin V-FITC
I
si-NC
si-STXBP1-1
Apoptosis rate (%)
U251
U87

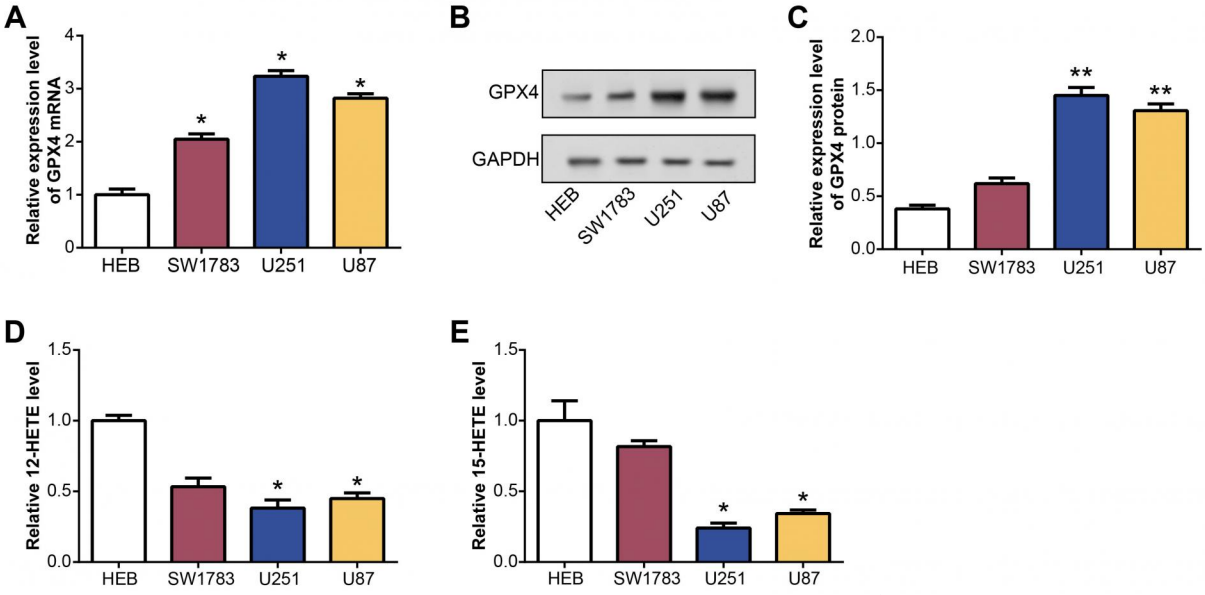
A
Relative expression level of GPX4 mRNA
0
1
2
3
4
*
*
*
HEB
SW1783
U251
U87
B
GPX4
GAPDH
HEB
SW1783
U251
U87
C
Relative expression level of GPX4 protein
0.0
0.5
1.0
1.5
2.0
**
**
HEB
SW1783
U251
U87

D
Relative 12-HETE level
0.0
0.5
1.0
1.5
*
*
HEB
SW1783
U251
U87
E
Relative 15-HETE level
0.0
0.5
1.0
1.5
*
*
HEB
SW1783
U251
U87

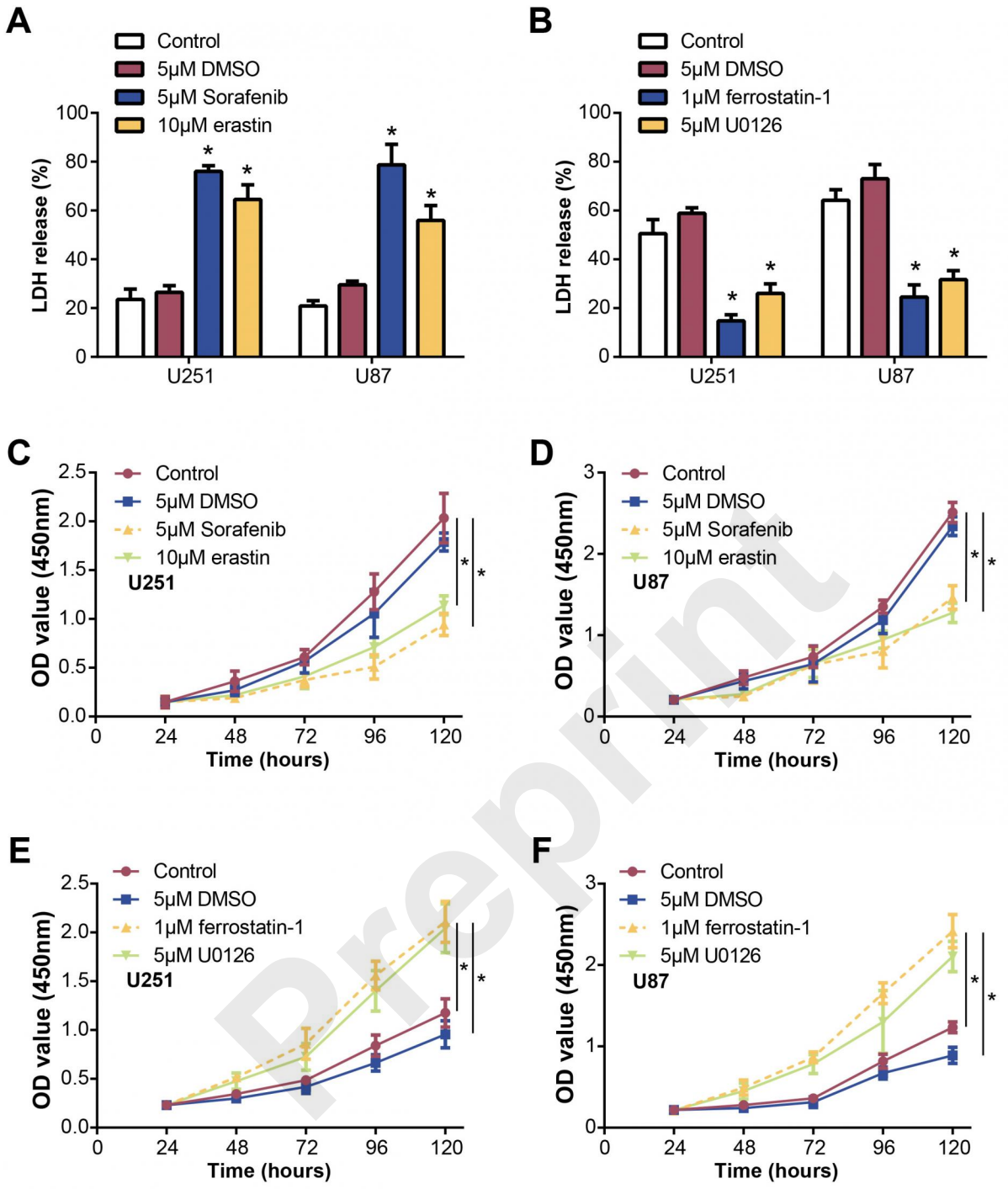
A
Control
5μM DMSO
5μM Sorafenib
10μM erastin
LDH release (%)
U251
U87
B
Control
5μM DMSO
1μM ferrostatin-1
5μM U0126
LDH release (%)
U251
U87
C
Control
5μM DMSO
5μM Sorafenib
10μM erastin
U251
OD value (450nm)
Time (hours)
D
Control
5μM DMSO
5μM Sorafenib
10μM erastin
U87
OD value (450nm)
Time (hours)
E
Control
5μM DMSO
1μM ferrostatin-1
5μM U0126
U251
OD value (450nm)
Time (hours)
F
Control
5μM DMSO
1μM ferrostatin-1
5μM U0126
U87
OD value (450nm)
Time (hours)

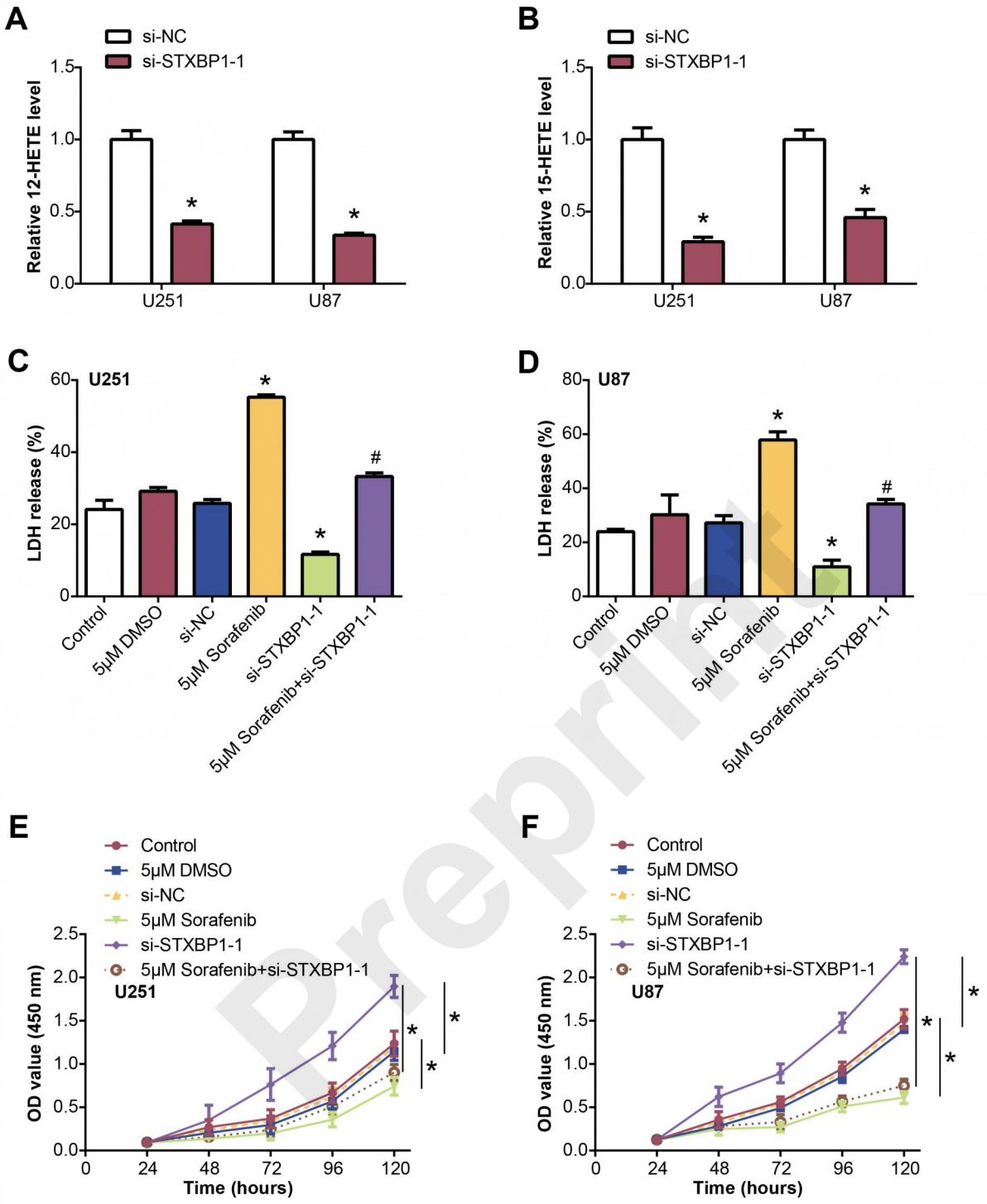
A
si-NC
si-STXBP1-1
Relative 12-HETE level
1.5
1.0
0.5
0.0
*
*
U251
U87
B
si-NC
si-STXBP1-1
Relative 15-HETE level
1.5
1.0
0.5
0.0
*
*
U251
U87
C
U251
LDH release (%)
60
40
20
0
*
*
#
Control
5μM DMSO
si-NC
5μM Sorafenib
si-STXBP1-1
5μM Sorafenib+si-STXBP1-1
D
U87
LDH release (%)
80
60
40
20
0
*
*
#
Control
5μM DMSO
si-NC
5μM Sorafenib
si-STXBP1-1
5μM Sorafenib+si-STXBP1-1
E
Control
5μM DMSO
si-NC
5μM Sorafenib
si-STXBP1-1
5μM Sorafenib+si-STXBP1-1
U251
OD value (450 nm)
2.5
2.0
1.5
1.0
0.5
0.0
0
24
48
72
96
120
Time (hours)
*
*
*
F
Control
5μM DMSO
si-NC
5μM Sorafenib
si-STXBP1-1
5μM Sorafenib+si-STXBP1-1
U87
OD value (450 nm)
2.5
2.0
1.5
1.0
0.5
0.0
0
24
48
72
96
120
Time (hours)
*
*
*

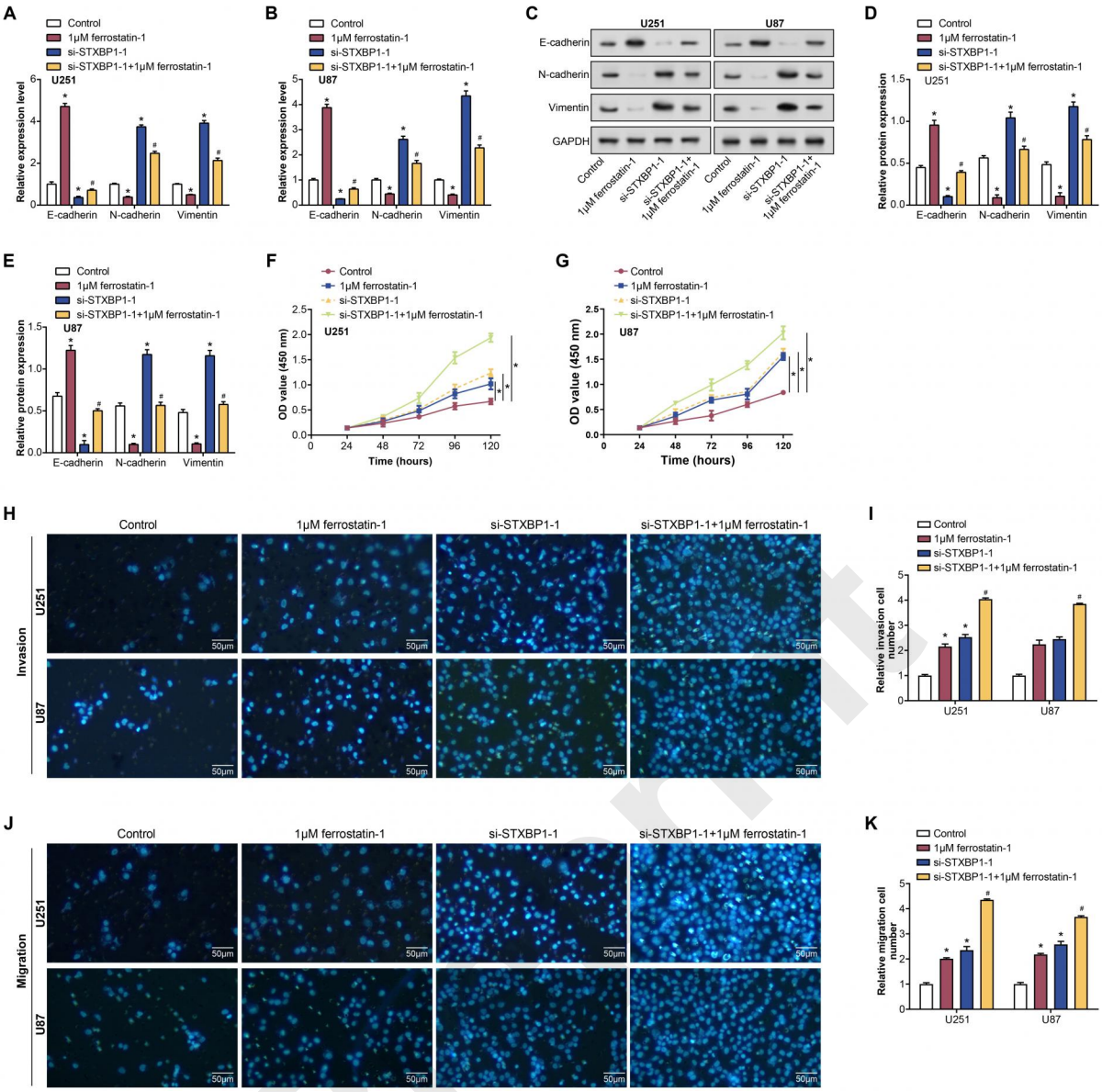
A
Control
1μM ferrostatin-1
si-STXBP1-1
si-STXBP1-1+1μM ferrostatin-1
U251
Relative expression level
E-cadherin
N-cadherin
Vimentin
B
U87
C
U251
U87
E-cadherin
N-cadherin
Vimentin
GAPDH
D
Relative protein expression
E
F
OD value (450 nm)
Time (hours)
G
H
Invasion
I
Relative invasion cell number
J
Migration
K
Relative migration cell number
50μm